Seitz, F.: Atmospheric and oceanic influences on polar motion - numerical results from two independent model combinations.

Artificial Satellites, Vol. 40, Nr. 3, pp 199-215, ISSN 0208-841X, 2005.

ARTIFICIAL SATELLITES, Vol. 40, No.3,
199-215, ISSN 0208-841X, 2005.

Atmospheric and oceanic influences on polar motion - numerical results from two independent model combinations

Florian Seitz
Deutsches Geodätisches Forschungsinstitut, München

Abstract

On seasonal to interannual time scales the largest fluctuations of Earth rotation are caused by atmospheric and oceanic mass redistributions. In this paper, the influence of these two subsystems on polar motion is discussed on the basis of numerical results of the dynamic Earth system model DyMEG. The model is forced by two independent but consistent combinations of atmospheric and oceanic angular momenta. The first combination comprehends atmospheric reanalyses of NCEP/NCAR in combination with the ocean circulation model ECCO. The second combination consists of the unconstrained atmosphere model ECHAM3 and the ocean model OMCT. Both forcing conditions differ conceptually: Since in ECCO an exactly inverse barometric response of the ocean to atmospheric pressure variations is assumed, pressure anomalies from NCEP are not used for the forcing of ECCO. In contrast, the pressure variations of ECHAM3 are taken into account by OMCT. Consequently the excitations of polar motion deduced from these model combinations differ as the pressure over the oceans is eliminated in NCEP but not in ECHAM3. Likewise, pressure variations do not influence the ocean circulation in ECCO but they yield a significant contribution to the circulation described by OMCT. The polar motion series produced by DyMEG with the differing forcing conditions are compared to each other in both the time and the frequency domain. In particular, the differing treatment of atmospheric pressure variations in both model combinations becomes obvious when atmospheric and oceanic forcing is applied to DyMEG separately. The results for polar motion from NCEP and ECCO feature significantly differing signal characteristics than the respective results with ECHAM3 and OMCT.

1 Introduction

Variations of Earth rotation are caused by the redistribution and motion of mass elements in various components of the Earth system which are caused by exogenous and endogenous forces. With respect to an Earth-fixed reference frame, changes of the direction of the rotation axis can be viewed as polar motion whereas changes of the angular velocity of the reference frame are associated with variations of length-of-day (ΔLOD). Today, fluctuations of Earth rotation can be observed by modern space geodetic techniques with high accuracy. As the observations describe the integral effect of all underlying influences, it is usually very difficult to relate particular variations with their individual causative processes.

In order to interpret the geodetic time series for polar motion and ΔLOD geophysically, i.e., to assess the contributions of individual components of the Earth system, independent approaches from theory and modelling are required. In this paper, the reaction of the Earth on gravitational and geophysical forcing is analysed, using the dynamic Earth system model DyMEG (Dynamic Model for Earth rotation and Gravity) (Seitz *et al.*, 2004). The focus is laid on the study of polar motion on seasonal to

interannual time scales where the largest effects are due to mass redistributions within the fluid components atmosphere and ocean.

The contributions of these two system components on Earth rotation have been addressed in many recent publications, (e.g. Chen *et al.*, 2000; Brzezinski *et al.*, 2002; Brzezinski, 2003; Gross *et al.*, 2003; Salstein, 2005). In the following it is studied, in which way the resulting time series for polar motion of DyMEG are influenced, when the model is forced by two independent atmospheric and oceanic model combinations which are characterised by profound conceptual differences. The first combination is based on the atmospheric reanalyses of NCEP/NCAR (*National Centers for Environmental Prediction/National Centers for Atmospheric Research*) (Kalnay *et al.*, 1996). In order to describe the redistributions and motions of mass elements in the atmosphere and in the oceans consistently, NCEP data is combined with the results of the global ocean circulation model ECCO (Stammer *et al.*, 2003). The ocean dynamics described by the unconstrained ECCO version c20010701, which is applied in this study, is computed from NCEP forcing fields comprising wind stress, heat and freshwater fluxes. The ocean's response to atmospheric pressure variations is assumed to be exactly inverse barometric (IB-hypothesis). Both models cover the epoch between 1.1.1980 and 1.3.2002. The second combination is based on the global atmospheric circulation model ECHAM3-T21 of the Deutsches Klimarechenzentrum (DKRZ) (DKRZ, 1992; Roeckner *et al.*, 1992). In contrast to the NCEP reanalyses, ECHAM3 is not assimilated but solely forced by observed monthly mean sea surface temperatures and ice coverages. The global ocean model for circulation and tides (OMCT) (Thomas *et al.*, 2001) is forced by ECHAM3 including atmospheric pressure variations. In contrast to the first combination, no inverse barometric (IB) correction is applied to the atmospheric pressure fields in ECHAM3 since atmospheric pressure forcing is taken into account by OMCT. The model combination ECHAM3-OMCT covers the period from 1.1.1975 until 31.12.1994.

2 Balance of angular momentum in the Earth system

DyMEG is based on the balance of angular momentum in the Earth system. With respect to a rotating reference system, the Earth's reaction on mass redistributions can be described by the Liouville differential equation (Munk and MacDonald, 1960):

$$\frac{d}{dt}\big(\,\mathbf{I}(t)\,\boldsymbol{\omega}(t)+\mathbf{h}(t)\,\big)+\boldsymbol{\omega}(t)\times\big(\,\mathbf{I}(t)\,\boldsymbol{\omega}(t)+\mathbf{h}(t)\,\big)=\mathbf{L}(t)\;. \tag{1}$$

In this equation, $\boldsymbol{\omega}(t)$ denotes the rotation vector of the terrestrial system with respect to an inertial system. Temporal variations of Earth rotation are interpreted as small deviations from a uniform rotation. In the terrestrial system, the coordinates of the Earth rotation vector are expressed by $\boldsymbol{\omega}(t) = \Omega\cdot[\,m_1(t), m_2(t), 1+m_3(t)\,]'$ where $\Omega = 2\pi/86164\,\mathrm{s}$ is the approximate angular velocity of the terrestrial system. Its z-axis is directed approximately towards the Earth's maximum moment of inertia C, its x-axis points towards the Greenwich meridian and its y-axis towards 90° E. The small dimensionless quantities m_i $(i=1,2,3)$ denote deviations of the instantaneous rotation axis from the uniform rotation. The variation of the direction of the rotation axis (polar motion) is described by $m_1(t)$ and $m_2(t)$. Fluctuations of the Earth's angular velocity are equivalent to variations of ΔLOD. They follow from the variation of the absolute value of the Earth rotation vector $|\boldsymbol{\omega}| \approx \Omega\,(1+m_3)$. The error due to this approximation is $10^{-16}\,\mathrm{s}$ and therefore negligible.

Gravitational forces of Sun and Moon cause mass redistributions in the atmosphere, the oceans and the solid Earth (McCarthy and Petit, 2003). Besides, the extraterrestrial bodies exert direct torques which are denoted by the vector $\mathbf{L}(t)$ (Lambeck, 1980). Non-gravitational geophysical and climate processes as well as the weather lead to additional displacements and motions of masses in the atmosphere, the ocean, and

other subsystems which are not regarded here. All mass redistributions have a direct effect on the balance of angular momentum, where they show up as changes of the Earth's tensor of inertia $\mathbf{I}(t)$ and angular momentum $\mathbf{h}(t)$ with respect to the rotating reference system. Besides, they load the Earth's body which results in deformations and gives rise to supplementary deviations of $\mathbf{I}(t)$. This so-called indirect effect is computed in DyMEG from atmospheric surface and oceanic bottom pressure fields via Green's functions (Farrell, 1972). Angular momentum exchanges between the Earth's core and mantle are not considered in the model. As they mainly contribute to sub-daily polar motion, the decoupling of these two system components is justified on seasonal to interannual time scales.

As a consequence of forced polar motion, the centrifugal potential of the Earth varies with time. This leads to additional mass redistributions (rotational deformations) in the system components. In DyMEG, rotational deformations of the solid Earth and the oceans are regarded (McCarthy and Petit, 2003). Atmospheric mass redistributions due to rotational variations are neglected. The rheology of the Earth and, therewith associated, the effect of forced rotational variations on the centrifugal potential of the Earth is parameterised in DyMEG by the complex Love number k_2 (Smith and Dahlen, 1981; Seitz *et al.*, 2004). Its imaginary part describes the loss of energy due to friction which leads to a damping of the free polar motion. Hence the Chandler amplitude of the model would diminish within a few decades, i.e. the Earth rotation axis would converge to the polar axis of inertia, in the absence of counteractive excitation mechanisms.

Solving the Liouville equation for $\boldsymbol{\omega}(t)$ leads to the variations of Earth rotation. In DyMEG, this coupled system of three first order differential equations is solved numerically as an initial value problem (Seitz *et al.*, 2004). This is in contrast to most of the previous studies, in which the equation is linearised and solved analytically (Munk and MacDonald, 1960; Lambeck, 1980). As a side effect of the non-linear procedure, the solution contains contributions of the tensor elements $\Delta I_{11}(t)$, $\Delta I_{22}(t)$, and $\Delta I_{12}(t)$, too. Their influence on polar motion will be addressed later in this paper (cf. 4.1). Within a sensitivity analysis of the model (Seitz and Kutterer, 2005) it was shown, that the solution by means of a Runge-Kutta-Fehlberg method of $4^{th}/5^{th}$ order is reliable from the algorithmic point of view. Initial values $m_i(t_0)$ are computed from the C04 series for polar motion and ΔLOD of the International Earth Rotation and Reference Systems Service (IERS) (Dick and Richter, 2004). The relation between the observations, hereafter denoted by $\tilde{x}(t)$ and $\tilde{y}(t)$, and $m_1(t)$ and $m_2(t)$ was described by (Gross, 1992). In the framework of the sensitivity analysis of DyMEG, the dependence of the numerical solution on the choice of the initial values $m_i(t_0)$ was assessed. The study showed that the modification of the initial values within an interval of $3\sigma_i$ around the respective C04 value (σ_i denotes the standard deviation of the observations within an interval of 30 days around the starting date $t = t_0$) does not have a large effect on the resulting polar motion as the results of 30 test runs with DyMEG showed very similar results (RMS differences among each other < 5 mas). Hence the comparison of the results with the geodetic observations is not limited by the choice of the initial conditions as long as the values are taken from a reasonable interval.

3 Atmospheric and oceanic forcing

3.1 Characterisation of the models

For the forcing of DyMEG, the two aforementioned atmosphere-ocean model combinations NCEP-ECCO and ECHAM3-OMCT are applied. Both model combinations are consistent representations of dynamics and mass redistributions in the subsystems ocean and atmosphere. However there are conceptual differences between the models which are of fundamental importance for the achievable results. The NCEP reanalyses are based on observed atmospheric and non-atmospheric data, such as winds, air

pressure, temperature, humidity, monthly mean sea surface temperatures, and ice coverages which have been analysed with the analysis schema of a weather forecast model (Kalnay *et al.*, 1996). The horizontal spatial resolution of the NCEP data set is 2,5° x 2,5°. Vertically it comprehends 17 layers between the Earth's surface and a (variable) height, in which the air pressure reaches 10 hPa. In combination with the coupled ocean circulation model ECCO, the reanalyses allow for a rather realistic description of the atmosphere-ocean dynamics. This refers especially to the (variable) frequency content and the amplitudes and phases of individual signal components. As the phases of modelled and real angular momentum variations are widely coherent as a consequence of the assimilation, one can expect a good correlation between the NCEP-ECCO model result for polar motion and the geodetic observations C04.

The global atmospheric general circulation model ECHAM3-T21 has been developed from a weather forecast model of the ECMWF (*European Centre for Medium Range Weather Forecasts*) and is run at the DKRZ in Hamburg (DKRZ, 1992). It has a horizontal spatial resolution of 5,625° x 5,625° and a vertical resolution of 19 layers from the surface up to the pressure level of 10 hPa. ECHAM3 is geared towards climate studies and does not assimilate atmospheric observations. The dynamics described by the model is exclusively based on monthly mean sea surface temperatures and ice coverages. Such a free model allows for comprehensive studies of the simulated atmospheric processes which can solely be explained by the model physics. It has been shown in several studies, that the model is capable of reproducing a realistic climate variability (Hense and Römer, 1995; Gualdi *et al.*, 1997; Hide *et al.*, 1997; Glowienka-Hense, 1999). But since ECHAM3 does not assimilate atmospheric data, simulated and real variations of angular momentum are not synchronised. Hence the phases of individual modelled signal components do not necessarily correspond to observations, although the general atmospheric variability is reproduced quite reasonably.

As stated above, none of the applied ocean models assimilates oceanographic observations. ECCO describes the world ocean between 78° N and 78° S and has a horizontal resolution of 1° x 1° which is densified in tropic regions to 0,3° x 0,3°. The distance of the vertical layers ranges from 10 m to 400 m. ECCO is driven by atmospheric wind stress, heat and freshwater fluxes from NCEP, but it does not regard the ocean's reaction to atmospheric pressure anomalies (IB-hypothesis). Accordingly it is assumed, that atmospheric pressure variations lead to an instantaneous isostatic reaction of the ocean surface without influencing its dynamics. As the ocean bottom pressure thereby remains unchanged, the IB-hypothesis is tantamount to the neglect of air pressure over the ocean and the assumption of an undeformed ocean surface. It has been shown, that in general the IB-assumption is justified on time scales which are larger than 10 days. However, the ocean circulation is significantly influenced by atmospheric pressure forcing on shorter time scales. The deflection of an exactly invers barometric ocean response is largest in coastal and arctic regions (which are not covered by ECCO). This dynamic effect accounts for up to 10-15% of the entire oceanic excitation energy (Ponte *et al.*, 1998; Thomas, 2002) and cannot be included in IB circulation models.

The horizontal resolution of OMCT is 1,875° x 1,875° between 90° N and 90° S. In the vertical, OMCT comprehends 13 layers, of which six describe the upper 240 meters of the ocean. The model is driven by ECHAM3 including atmospheric pressure forcing. Furthermore, the effect of loading and self-attraction of water is regarded, which is usually neglected in ocean circulation models. Analyses of the OMCT excitations for polar motion showed, that this mechanism is the third largest oceanic influence on Earth rotation after the general (thermohaline and wind-driven) circulation and the pressure driven circulation (Thomas *et al.*, 2001). Although OMCT is able to account for ocean tides and circulation simultaneously, the model run which is applied in this paper solely comprehends ocean circulation. The total effect of the angular momentum variations due to ocean tides on polar motion is more than one order of magnitude smaller than the effects from ocean circulation (Thomas *et al.*, 2001). Ocean tides influence Earth

rotation mainly on daily and subdaily time scales. The effects of long period ocean tides, such as M_f, M'_f (semi-monthly), M_m (monthly), S_{sa} (semi-annual) and S_a (annual) on polar motion are below 1 mas (Gross *et al.*, 2003) and therewith far below the present model accuracy (cf. 4.1).

The regard of atmospheric pressure forcing by OMCT and its disregard by ECCO should not lead to a significantly different polar motion of DyMEG when the combined effect of atmosphere and oceans is considered. As there is no IB-correction in ECHAM3 (i.e., the pressure over the oceans is not set to zero) it is expected, that simulated atmospheric and oceanic signals are out of phase and tend to compensate each other when both excitations are superposed. Since the ocean is coupled to the atmosphere in both model combinations, consistent momentum, heat, and mass fluxes at the atmosphere-ocean boundary are ensured. Consequently, the thermohaline, wind- and (in the case of ECHAM3) pressure-driven oceanic circulation is in concordance with the instantaneously observed (NCEP) or simulated (ECHAM3) atmospheric state.

3.2 Comparison of the excitations

Deviations of the tensor of inertia $\Delta I_{ij}(t)$ $(i, j = 1, 2, 3)$ are computed from atmospheric surface pressure and oceanic bottom pressure variations. Angular momenta $\mathbf{h}(t)$ arise from the motion of mass elements with respect to the terrestrial reference system and are thus linked to winds and ocean currents. Fig. 1 displays the time series of deviations of the tensor elements $\Delta I_{13}(t)$ and $\Delta I_{23}(t)$ for the epoch, in which all four models are available (1980 until 1994). The mean annual amplitudes are given together with the phases w.r.t. 1.1.1980 in Table 1. The remaining four elements of the tensor which are secondary for polar motion are not discussed here. The comparison of the time series shows, that the deviations which are deduced from ECHAM3 and OMCT are characterised by higher signal amplitudes than the corresponding components of NCEP and ECCO. Here the different treatment of the atmospheric pressure variations over

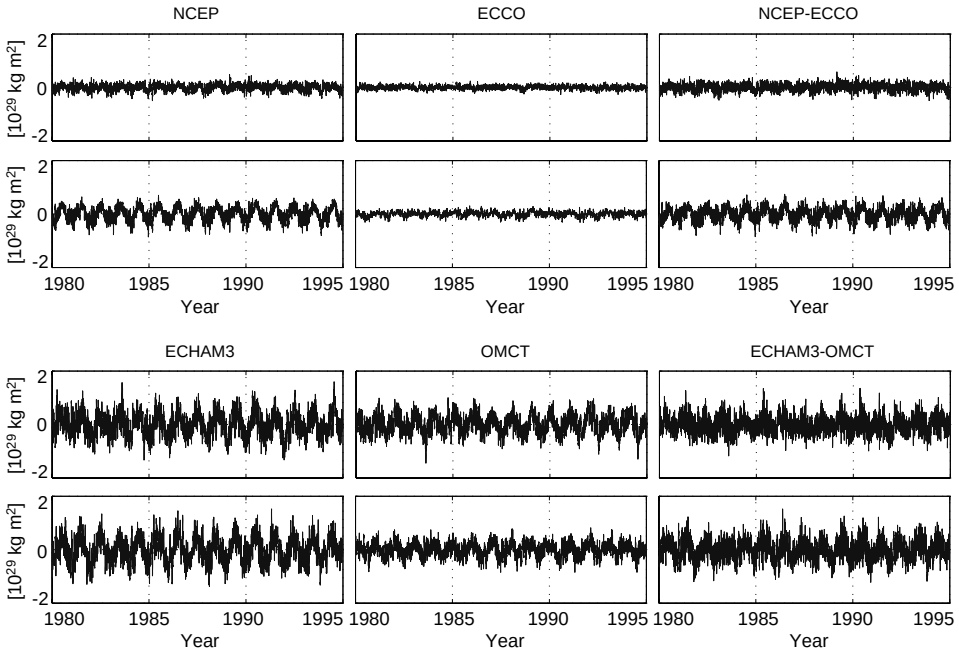

Figure 1: Temporal variations of the tensor elements $\Delta I_{13}(t)$ (respective top panel) and $\Delta I_{23}(t)$ (respective bottom panel) as described by the different atmosphere and ocean models in comparison with the corresponding combined effects.

	NCEP	ECCO	NCEP-ECCO
ΔI_{13}			
Amplitude [10^{29} kg m^2]	0,06	0,01	0,06
Phase [°]	272	88	273
ΔI_{23}			
Amplitude [10^{29} kg m^2]	0,26	0,06	0,20
Phase [°]	272	85	278
	ECHAM3	OMCT	ECHAM3-OMCT
ΔI_{13}			
Amplitude [10^{29} kg m^2]	0,37	0,30	0,17
Phase [°]	266	64	319
ΔI_{23}			
Amplitude [10^{29} kg m^2]	0,44	0,19	0,27
Phase [°]	277	83	292

Table 1: Mean annual oscillations in the time series of the atmospheric and oceanic tensor variations.

the oceans becomes obvious: Due to the IB-assumption of ECCO, the NCEP pressure fields are reduced by the pressure over the oceans (IB-correction). As OMCT explicitly regards atmospheric pressure forcing, atmospheric and oceanic angular momenta can be superposed consistently without any correction. Hence, the full atmospheric pressure effect is contained in the displayed time series of ECHAM3. The reduction of the atmospheric pressure in NCEP leads to a diminution of stochastic signals (noise) which are caused by random weather variations.

Analogously, the oceanic induced tensor variations reflect the differing treatment of atmospheric pressure by the ocean models. OMCT shows an annual signal which in both components has the same order of magnitude as the respective ECHAM3 signal. In contrast, the annual oscillation in ECCO is one order of magnitude weaker than in NCEP. As OMCT is linked to ECHAM3, the stronger stochastic atmospheric signal is also transferred into the ocean. The annual atmospheric variability of ECHAM3 is stronger in the component $\Delta I_{23}(t)$ whereas the annual oceanic signal of OMCT is stronger in $\Delta I_{13}(t)$. This is a consequence of the land/water distribution on the Earth. The regions which are most effective for $\Delta I_{13}(t)$ are located in the East Atlantic and the Central Pacific. Oceanic contributions to $\Delta I_{23}(t)$ predominantly originate from the Indian Ocean and the South-East Pacific and are small compared with the oceanic influences on $\Delta I_{13}(t)$. The component $\Delta I_{23}(t)$ is mainly affected by atmospheric mass redistributions over the North and South American continents as well as in Central Asia (Nastula and Salstein, 1999). Due to the IB-correction, NCEP features a low signal in $\Delta I_{13}(t)$. Since ECCO is not driven by atmospheric pressure, both annual amplitudes are much weaker than in OMCT.

The phases of the annual signals from the reanalyses are identical in both components, whereas a difference of 13° (which corresponds to approximately two weeks) shows up between $\Delta I_{13}(t)$ and $\Delta I_{23}(t)$ from ECHAM3. Due to the linkage of the ocean to the atmosphere, also the respective phases of ECCO agree better than the phases of OMCT. But in both model combinations, the oceanic and atmospheric annual oscillations are nearly out of phase. The discrepancy between an exact paraphase is smaller in the case of NCEP-ECCO (184° and 187°) than in the case of ECHAM3-OMCT (202° and 194°). Consequently the reaction of OMCT to the ECHAM3 forcing is not

exactly inverse barometric. As stated above, the largest deflections of an exactly invers barometric ocean response may occur in coastal and arctic regions (Thomas, 2002). It has been expected that the simulated atmospheric and oceanic signals compensate each other partially when ECHAM3 and OMCT are superposed. In fact, only the component $\Delta I_{23}(t)$ of the combined effects of NCEP-ECCO and ECHAM3-OMCT look rather similar. For $\Delta I_{13}(t)$ both the amplitude and the phase of ECHAM3-OMCT clearly differ from the values determined for NCEP-ECCO. Obviously, the annual signal of the unconstrained model combination ECHAM3-OMCT seems to be overestimated in this component.

In Fig. 2 the variations of $h_1(t)$ and $h_2(t)$ are displayed. Both atmospheric components are characterised by strong noise, which is due to stochastic weather variations and associated local winds (Weickmann *et al.*, 2000). While ECHAM3 does not show significant annual variability, $h_2(t)$ of the reanalyses is characterised by a glaring oscillation with an amplitude of $0,33 \cdot 10^{25}$ kg m^2 s^{-1}. This signal is caused by a vast overestimation of winds over continents on seasonal time scales (Kalnay *et al.*, 1996; Aoyama and Naito, 2000) and does not correspond to reality. The ocean's contribution to $h_1(t)$ and $h_2(t)$ is comparatively minor. For ECCO as well as for OMCT both signal components are rather noisy. Due to the stochastic character of the wind fields, the coupling of the ocean to the atmosphere yields currents which do not show significant periodic variations. The signal amplitudes of OMCT which are almost twice as large as the amplitudes of ECCO can be ascribed to the effects of loading and self-attraction and atmospheric pressure forcing, which lead to additional balancing currents. The sum of atmospheric and oceanic angular momenta features slightly stronger signal amplitudes in the case of ECHAM3-OMCT. But the departure of the combined angular momentum series of both model combinations from each other is - apart from the artificial annual signal caused by NCEP - smaller than the departure of the respective tensor elements.

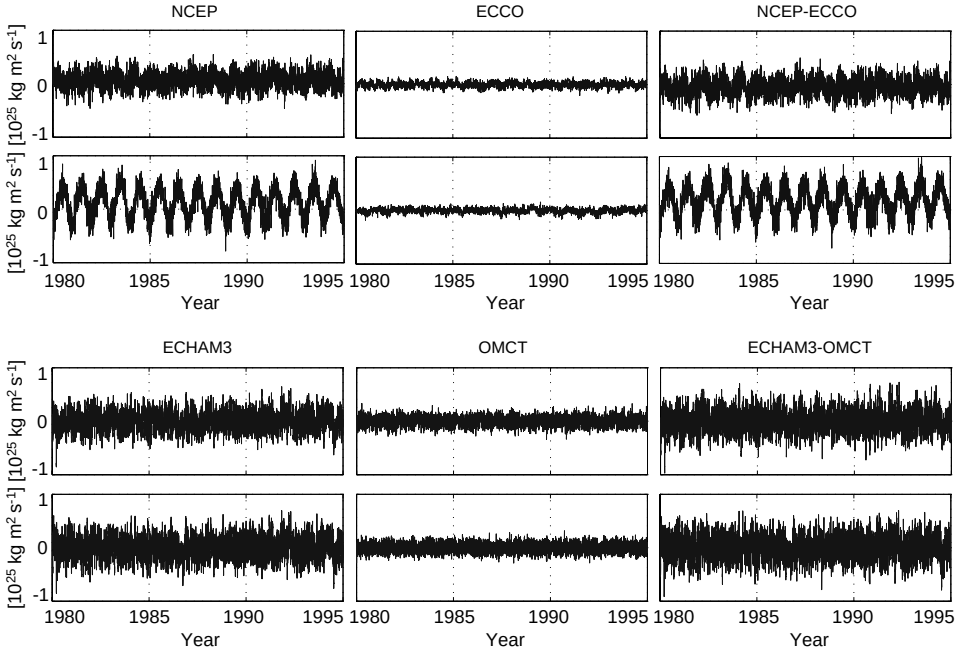

Figure 2: Temporal variations of angular momenta $h_1(t)$ (respective top panel) and $h_2(t)$ (respective bottom panel) as described by the different atmosphere and ocean models in comparison with the corresponding combined effects.

4 Results for polar motion

4.1 Combined atmospheric and oceanic effect

For each of the model combinations a run with DyMEG is performed. The results (Fig. 3) cover the time frames between 1.1.1980 and 1.3.2002 (NCEP-ECCO) and between 1.1.1975 and 31.12.1994 (ECHAM3-OMCT). For comparison the geodetic observations $\tilde{x}(t)$ and $\tilde{y}(t)$ are displayed (linear trends have been removed from all curves). While the NCEP-ECCO run agrees very well with the C04 series in both components, ECHAM3-OMCT yields a result which shows an increased beat amplitude. Tables 2 (NCEP-ECCO) and 3 (ECHAM3-OMCT) compile the mean amplitudes and the phases w.r.t. the starting date of the two largest signal components, i.e., the annual and the Chandler oscillation, which were simultaneously estimated by least squares adjustment. The values are contrasted to results from the C04 series for the respective epoch. Correlation coefficients and RMS differences are additionally provided.

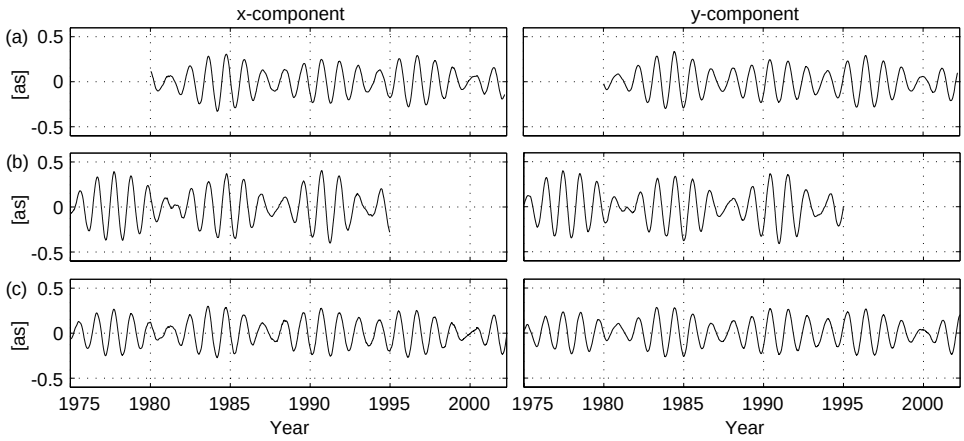

Figure 3: Model results for polar motion for combined atmospheric and oceanic forcing. (a) NCEP-ECCO (b) ECHAM3-OMCT, (c) geodetic observations C04. Linear trends have been removed.

The phases of model results and observations agree well and the divergence is mostly less than one week. The only exception is the annual signal of the x-component of the NCEP-ECCO run which shows a phase shift of -17 days compared to the observations. The amplitudes of NCEP-ECCO feature only small deviations from C04. This is in contrast to a recent study by Gross *et al.* (2003) which is based on the same atmosphere-ocean combination. In their analyses they obtained almost identical values for the observed polar motion amplitudes during 1980 and 2000 (x-component: 80,2 mas; y-component: 73,4 mas), but they found that the combined effect of atmosphere and oceans is only capable of explaining 69,0 mas and 60,4 mas respectively. The model time series for ECHAM3-OMCT is characterised by an annual signal which is rather twice as large than observed. This might result from the overestimated annual variability in $\Delta I_{13}(t)$ (cf. 3.2). As the forced polar motion is coupled back to the Chandler wobble via rotational deformations and mantle anelasticity, the mean amplitude of the free polar motion of DyMEG is likewise enhanced.

In order to study the time-variable character of the time series, a wavelet analysis based on the Morlet wavelet (Schmidt, 2001) is performed for both results as well as for the residuals between the polar motion from DyMEG and the geodetic observations (Fig. 4). On the right hand side of the scalograms the normalised wavelet coherence is displayed. The coherence reflects the agreement of the energy content between model result and observation depending on the frequency. For NCEP-ECCO, nearly no signal

	NCEP-ECCO		C04 (1980-2002)	
	x-component	y-component	x-component	y-component
Correlation with C04	0,98	0,99	-	-
RMS difference [mas]	29,5	23,3	-	-
Annual oscillation				
Amplitude [mas]	85,4	79,1	81,7	75,4
Phase [°]	199	303	215	306
Phase shift [days]	-17	-3	-	-
Chandler oscillation				
Amplitude [mas]	185,7	186,5	179,5	179,4
Phase [°]	92	184	99	189
Phase shift [days]	-7	-6	-	-

Table 2: Comparison of the model results for NCEP-ECCO with the observations (1980-2002).

	ECHAM3-OMCT		C04 (1975-1994)	
	x-component	y-component	x-component	y-component
Correlation with C04	0,95	0,94	-	-
RMS difference [mas]	70,8	75,8	-	-
Annual oscillation				
Amplitude [mas]	167,7	167,9	85,0	76,2
Phase [°]	201	295	208	299
Phase shift [days]	-7	-5	-	-
Chandler oscillation				
Amplitude [mas]	202,9	201,7	173,7	173,5
Phase [°]	0	91	355	89
Phase shift [days]	5	3	-	-

Table 3: Comparison of the model results for ECHAM3-OMCT with the observations (1975-1994).

energy is visible in the prograde scalogram of the residuals. Minor discrepancies occur between 1985 and 1988 as well as between 1995 and 2000 in the annual band, where the energy of the model results departs about 2% from the energy of the observations. Consequently the corresponding coherence points out an almost perfect agreement. The retrograde spectrum (note the different scaling) shows an annual signal which is one order of magnitude larger than observed. This discrepancy can possibly be explained by the above mentioned phase shift of -17 days between the x-components of the model result and C04 and leads to a lower coherence of the retrograde signals.

For ECHAM3-OMCT the largest deviations between the model time series and the observations occur in the prograde annual band. This discrepancy is maximum during the first years of the integration but decreases with time. The Chandler energy of the model result tends to increase over the years. The prograde scalogram of the residuals does not feature energy in the Chandler band between 1975 and 1988 which suggests, that the increase of the Chandler amplitude corresponds to reality between 1975 and 1988. But afterwards some energy in the scalogram becomes obvious in a band around 430 days. Hence, the Chandler wobble of DyMEG is excited too much by ECHAM3-OMCT after 1988. As for NCEP-ECCO, the coherence shows good agreement for the prograde range between 300 and 500 days. The retrograde scalogram of the residuals is

characterised by some energy in the annual band which is, however, about two-thirds smaller than in the respective scalogram of the residuals for NCEP-ECCO. Like in the prograde scalogram, the discrepancy between the retrograde annual oscillations of model and C04 is largest at the beginning of the time series but decreases towards the end.

The wavelet analysis reveals that the annual oscillation of NCEP-ECCO is more elliptic than observed. In contrast, the characteristics of the annual signal of ECHAM3-OMCT is - apart from its amplitude - in good agreement with C04. For the latter combination, the relation of the values in the pro- and retrograde scalograms of model result and observations (not shown) is similar. In the prograde Chandler band, the scalograms do not show major (NCEP-ECCO) or only temporary (ECHAM3-OMCT) discrepancies. Hence both model combinations are able to counteract the damping of the Earth's free polar motion which is due to mantle dispersion (Seitz *et al.*, 2004). The Chandler wobble is well explained by the sum of atmospheric and oceanic effects. Especially the (more realistic) result with NCEP-ECCO implies that (apart from errors

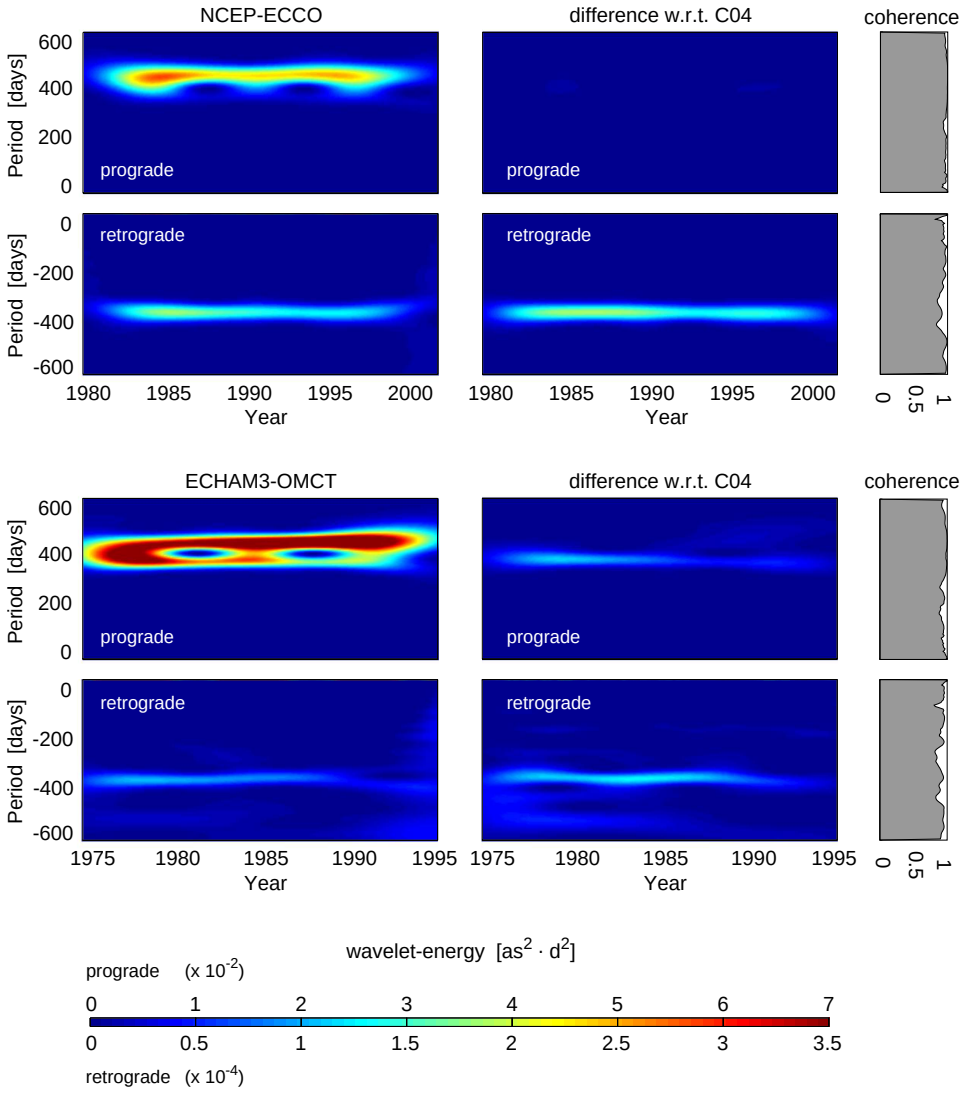

Figure 4: Wavelet scalograms of the model results and the residuals w.r.t the observations. Top: NCEP-ECCO, bottom: ECHAM3-OMCT.

in the atmospheric and oceanic data) other excitation mechanisms, such as hydrologic effects are secondary contributors to the free polar motion. However they seem to be important for the annual oscillation which is not reproduced just as well.

As the Liouville equation is solved numerically in DyMEG, the influences of the tensor elements which are usually neglected in the analytical approach due to linearisation (Lambeck, 1980) are contained in the solution, too (cf. 2). Their influence on polar motion is assessed by comparing the above model run for ECHAM3-OMCT in which these elements are considered with a run in which they are neglected. This experiment results in a RMS difference of 3 mas for both components of polar motion. Although this is far below the present model accuracy, the effect is larger than the accuracy of modern space geodetic techniques.

4.2 Separated atmospheric and oceanic effects

In order to study the individual contributions of the ocean and the atmosphere to polar motion and to compare the atmospheric and oceanic models to each other, a separated run with DyMEG is performed for each of the models. All simulations span the epoch between 1.1.1980 and 31.12.1994 which is covered by the four models. This is done in order to avoid discrepancies between the time series which might result from differing initial conditions and thus could lead to misinterpretations. The model results for the x-component of polar motion are shown in Fig. 5. As for combined atmospheric and oceanic excitation, the y-components look alike.

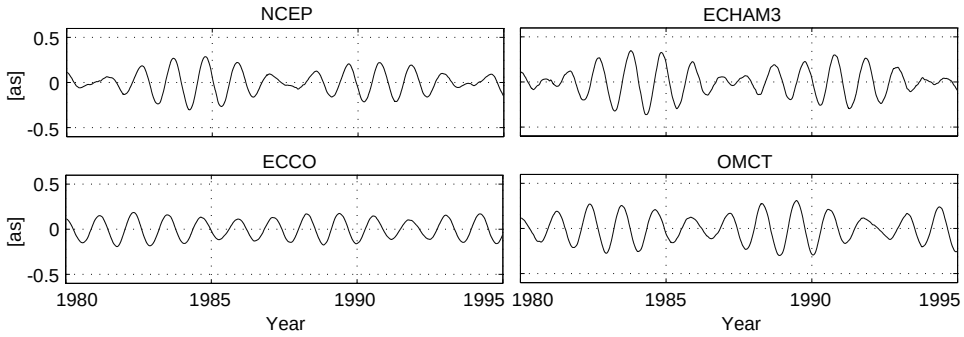

Figure 5: Model results for separated atmospheric and oceanic forcing (x-components). Linear trends have been removed.

Tables 4 (NCEP and ECHAM3) and 5 (ECCO and OMCT) compile the amplitudes and phases of the respective atmospheric and oceanic induced annual and Chandler oscillations. Besides, the resulting mean Chandler periods as derived from a Fourier transform are provided. They differ partially a few days from the Chandler period which has been determined from the C04 series for this epoch (432,5 days). Moreover, they depart from the mean Chandler periods of the respective combined model runs (NCEP-ECCO: 433,1 days; ECHAM3-OMCT: 432,4 days). Here the sensitivity of the numerical system with respect to the excitations becomes obvious, as modified resonance conditions lead to significant effects on the free polar motion.

Due to the IB-correction that has been applied to the NCEP pressure fields, the annual oscillation of the NCEP run is significantly weaker than the one produced by ECHAM3. Analogously, OMCT which regards pressure forcing leads to a much higher ocean induced annual polar motion than ECCO (cf. Fig 1). Obviously, the ocean's contribution to the y-component of polar motion is stronger than it is to the x-component. Conversely, the atmosphere causes stronger annual variations in the direction of the x-axis than in the direction of the y-axis. The relation between the annual amplitudes of x- and y-component agrees well for both ocean models. However, the forcing with

	NCEP		ECHAM3	
	x-component	y-component	x-component	y-component
Annual oscillation				
Amplitude [mas]	111,6	100,2	158,7	152,9
Phase [°]	193	289	186	272
Chandler oscillation				
Amplitude [mas]	146,4	147,2	136,4	135,8
Phase [°]	82	174	36	128
Period [days]	431,5	432,6	430,4	430,7

Table 4: Comparison of annual and Chandler oscillations of the model results for atmospheric forcing.

	ECCO		OMCT	
	x-component	y-component	x-component	y-component
Annual oscillation				
Amplitude [mas]	29,6	33,1	92,7	100,1
Phase [°]	14	66	306	23
Chandler oscillation				
Amplitude [mas]	132,2	132,3	192,1	193,0
Phase [°]	114	204	119	213
Period [days]	433,5	433,7	436,6	437,4

Table 5: Comparison of annual and Chandler oscillations of the model results for oceanic forcing.

ECHAM3 leads to a smaller discrepancy between both components than the forcing with NCEP.

The comparison of the phases of the annual polar motion shows, that the results for NCEP and ECCO are out of phase. Especially in the x-component the paraphase is almost exact. But the phase relations of ECHAM3 and OMCT differ from this behaviour. As it was stated above (cf. 3.2), the reaction of OMCT to atmospheric pressure forcing was found to be not exactly invers barometric.

The prograde wavelet scalograms of the results for the two atmosphere models and for OMCT (Fig. 6) feature rather stable signal energy in the annual band. The prograde scalogram of ECCO does not show a strong annual oscillation. As the pressure variations of ECHAM3 are not partially compensated by the ocean in this separated model run, the prograde annual polar motion from ECHAM3 is even stronger than the Chandler oscillation. Both ECHAM3 and OMCT also lead to conspicuous retrograde annual oscillations which tend to attenuate each other when both models are applied simultaneously (cf. Fig. 4). The Chandler oscillation which influences solely the prograde spectrum of polar motion is particularly excited by the oceanic excitations. For ECCO, its signal energy is almost invariable throughout. The result for OMCT features a slight increase of the energy towards the end of the simulation whereas the Chandler energy seems to decrease slightly with time in both atmospheric runs.

The experiments with separated atmospheric and oceanic forcing show, that both subsystems contribute essentially to polar motion. But the excitations described by different models depart significantly from each other which is - besides from model errors - especially founded in the consideration of different forcing mechanisms of atmospheric and oceanic variability. Hence the use of consistently coupled models for the description of the atmosphere and ocean dynamics is indispensable in order to include the necessary

compensations and thus to avoid artificial contributions resulting from unreal phase lags between physical processes in both subsystems.

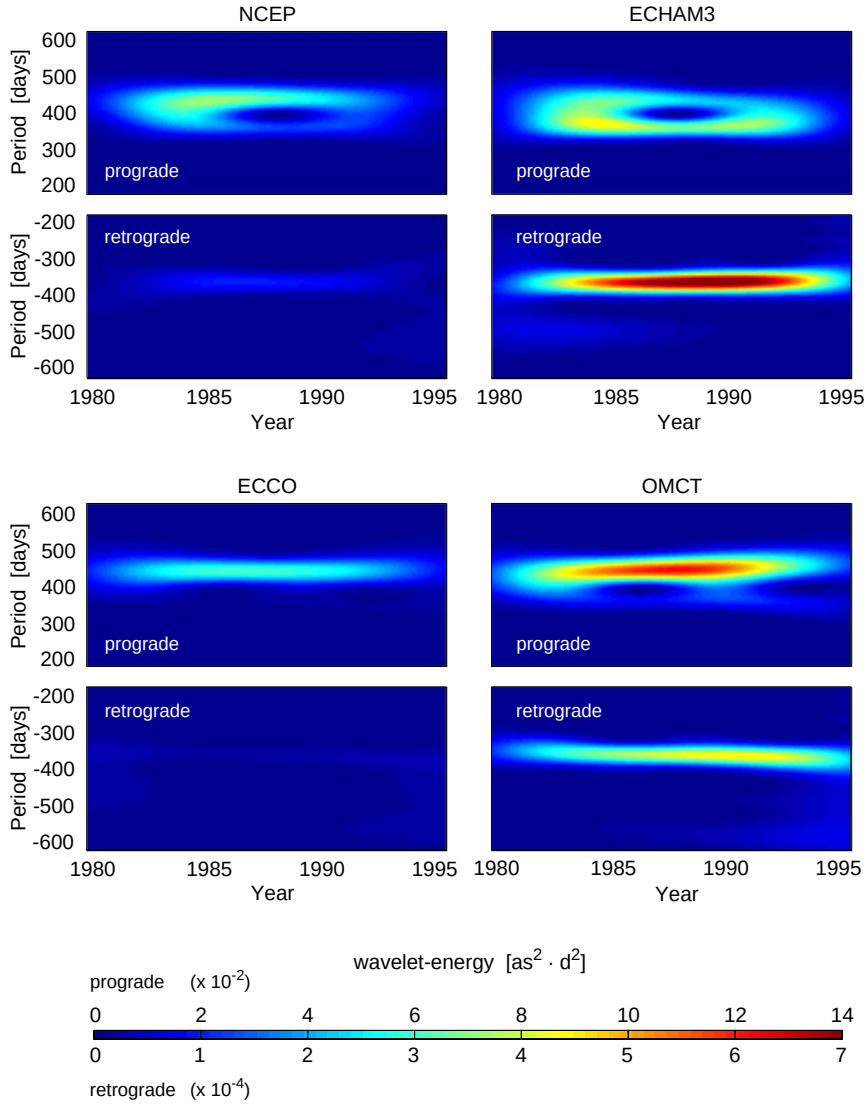

Figure 6: Wavelet scalograms of the model results for separated atmospheric and oceanic forcing.

5 conclusions

The results of DyMEG with separated atmospheric and oceanic forcing show significant discrepancies due to the IB assumption in NCEP-ECCO and the regard of atmospheric pressure forcing in ECHAM3-OMCT. The latter models lead to larger signal amplitudes than NCEP and ECCO. But when the excitations are introduced into the dynamic model simultaneously, the counteracting signals of ECHAM3 and OMCT tend to compensate each other partially. If the reaction of OMCT to atmospheric pressure variations would be exactly inverse barometric (and if all models were free of errors), the results of NCEP-ECCO and ECHAM3-OMCT should resemble each other. In other words, the differing handling of the pressure anomalies over the oceans should not influence the

results when the corresponding models are combined since the pressure induced oceanic variability would be compensated by the atmosphere. However, the results of NCEP-ECCO and ECHAM3-OMCT show conspicuous deviations from each other which are, of course, for the largest part due to errors in the atmospheric and oceanic data sets. Only a small part of the discrepancy might be due to the deviation of the ocean from the inverse barometric response which cannot be reproduced by ECCO. Due to the different concepts of the atmospheric excitations (data assimilation in NCEP, no data assimilation in ECHAM3) and errors in the models, e.g. the overestimation of winds in NCEP and the overestimation of the annual atmospheric variability in ECHAM3-OMCT, none of the data can be viewed as an ideal representative of the reality. As the errors of the atmospheric data are transferred into the ocean models, which on their part are erroneous, too, the combined effects of NCEP-ECCO and ECHAM3-OMCT can hardly be compared with respect to the influence of the IB/non-IB assumption.

Acknowledgments

This paper was developed within a project supported by DFG grant DR 143/12-1. ECHAM3 data was provided by DKRZ; OMCT simulations were performed by Dr. M. Thomas, TU Dresden; NCEP reanalyses were made available from the NOAA-CIRES Climate Diagnostics Center; ECCO data is a contribution of the Consortium for Estimating the Circulation and Climate of the Ocean funded by the National Oceanographic Partnership Program.

References

Aoyama, Y., I. Naito, 2000. Wind contributions to the Earth's angular momentum budgets in seasonal variation, *J. Geophys. Res.*, 105, 12417-12431.

Brzezinski, A., 2003. Oceanic excitation of polar motion and nutation - an overview, in: Proceedings of the IERS Workshop on Combination Research and Global Geophysical Fluids, eds. B. Richter, W. Schwegmann, W.R. Dick, IERS Technical Note No. 30, Verlag des Bundesamts für Kartographie und Geodäsie, Frankfurt am Main, 144-149.

Brzezinski, A., C. Bizouard, S.D. Petrov, 2002. Influence of the atmosphere on earth rotation: What can be learned from the recent atmospheric angular momentum estimates?, *Surveys in Geophysics*, 23, 33-69.

Chen, J.L., C.R. Wilson, B.F. Chao et al., 2000. Hydrological and oceanic excitations to polar motion and length-of-day variations, *Geophys. J. Int*, 141, 149-156.

Dick, W.R., B. Richter (Eds.), 2004. IERS Annual Report 2003, Verlag des Bundesamts für Kartographie und Geodäsie, Frankfurt am Main.

Deutsches Klimarechenzentrum (DKRZ), 1992. *The ECHAM3 atmospheric general circulation model*, Tech. Rep. 6, Hamburg.

Farrell, W., 1972. Deformation of the Earth by surface loads, *Rev. Geophys. Space Phys.*, *10*, 761-797.

Glowienka-Hense, R., 1999. Forced and free variability of the semi-annual wave in the ECHAM GCM, *Climate Dynamics*, 15, 269-275.

Gross, R.S., I. Fukimori, D. Menemenlis, 2003. Atmospheric and oceanic excitation of the Earth's wobbles during 1980-2000, *J. Geophys. Res.*, 108, doi:10.1029/2002JB002143.

Gross, R.S., 1992. Correspondence between theory and observations of polar motion, *Geophys. J. Int.*, 109, 162-170.

Gualdi, S., A. Navarra, H. von Storch, 1997. Tropical intraseasonal oscillation appearing in operational analyses and in a family of general circulation models, *J. Atm. Sci.*, 54, 1185-1202.

Hense, A., U. Römer, 1995. Statistical analysis of tropical climate anomaly simulations, *Climate Dynamics*, 11, 178-192.

Hide, R., J.O. Dickey, S.L. Marcus et al., 1997. Atmospheric angular momentum fluctuations during 1979-1988 simulated by global circulation models, *J. Geophys. Res.*, 102, 16423-16438.

Kalnay, E., M. Kanamitsu, R. Kistler et al., 1996. The NCEP/NCAR 40-Year Reanalysis Project, *Bull. Amer. Meteor. Soc.*, 77, 437-471.

Lambeck, K., 1980. *The Earth's variable rotation: Geophysical causes and consequences*, Cambridge University Press, New York.

McCarthy, D.D., G. Petit (Eds.), 2003. *IERS Conventions 2003*, IERS Technical Note 32, Verlag des Bundesamts für Kartographie und Geodäsie, Frankfurt am Main.

Munk, W.H., G.J.F. MacDonald., 1960. *The rotation of the Earth: A geophysical discussion*, Cambridge University Press, New York.

Nastula, J., D.A. Salstein, 1999. Regional atmospheric angular momentum contributions to polar motion excitation, *J. Geophys. Res.*, 104, 7347-7358.

Ponte, R.M., D. Stammer, J. Marshall, 1998. Oceanic signals in observed motions of the Earth's pole of rotation, *Nature*, 391, 476-479.

Roeckner, E., K. Arpe, L. Bengtsson et al., 1992. *Simulation of the present-day climate with the ECHAM model: Impact of the model physics and resolution*, Techn. Rep. 93, Max-Planck-Institut für Meteorologie, Hamburg.

Salstein, D., 2005. Earth rotation/polar motion excitations from atmospheric models, *Artificial Satellites*, 40(1), 35-46.

Schmidt, M., 2001. Wavelet analysis of stochastic signals, in: *High frequency to subseasonal variations in Earth rotation*, eds. B. Kolaczek, H. Schuh, D. Gambis, IERS Technical Note 28, Observatiore de Paris, 65-72.

Seitz, F., J. Stuck, M. Thomas, 2004. Consistent atmospheric and oceanic excitation of the Earth's free polar motion *Geophys. J. Int.*, 157, 25-35.

Seitz, F., H. Kutterer, 2005. Sensitivity analysis of the non-linear Liouville equation, in: *A Window on the Future of Geodesy*, ed. F. Sansó, IAG Symposia 128, Springer, Berlin, 601-606.

Smith, M.L., F.A. Dahlen, 1981. The period and Q of the Chandler wobble, *Geophys. J. R. astr. Soc.*, 64, 223-281.

Stammer, D., C. Wunsch, R. Giering et al., 2003. Volume, heat and freshwater transports of the global ocean circulation 1993-2000, estimated from a general circulation model constrained by World Ocean Circulation Experiment (WOCE) data, *J. Geophys. Res.*, 108, 10.1029/2001JC001115.

Thomas, M., 2002. *Oceanic induced variations of Earth rotation* (in German), PhD-thesis, Faculty of Geosciences, Universität Hamburg.

Thomas, M., J. Sündermann, E. Maier-Reimer, 2001. Consideration of ocean tides in an OGCM and impacts on subseasonal to decadal polar motion excitation, *Geophys. Res. Lett.*, 28(12), 2457-2460.

Weickmann, K.M., W.A. Robinson, M.C. Penland, 2000. Stochastic and oscillatory forcing of global atmospheric angular momentum, *J. Geophys. Res.*, 105, 15543-15557.

Received: 2005-06-08
Reviewed: 2005-07-29
Accepted: 2005-08-01